European Journal of Nuclear Medicine and Molecular Imaging (2019) 46:2077–2089
https://doi.org/10.1007/s00259-019-04399-0

ORIGINAL ARTICLE

[^{18}F]GTP1 (Genentech Tau Probe 1), a radioligand for detecting neurofibrillary tangle tau pathology in Alzheimer's disease

Sandra Sanabria Bohórquez[1] · Jan Marik[2] · Annie Ogasawara[2] · Jeff N. Tinianow[2] · Herman S. Gill[2] · Olivier Barret[3] · Gilles Tamagnan[3,4] · David Alagille[3,4] · Gai Ayalon[5] · Paul Manser[6] · Thomas Bengtsson[6] · Michael Ward[7,8] · Simon-Peter Williams[2] · Geoffrey A. Kerchner[7] · John P. Seibyl[3] · Kenneth Marek[3] · Robby M. Weimer[2,5]

Received: 20 November 2018 / Accepted: 11 June 2019 / Published online: 28 June 2019

Abstract

Objective Neurofibrillary tangles (NFTs), consisting of intracellular aggregates of the tau protein, are a pathological hallmark of Alzheimer's disease (AD). Here we report the identification and initial characterization of Genentech Tau Probe 1 ([^{18}F]GTP1), a small-molecule PET probe for imaging tau pathology in AD patients.

Methods Autoradiography using human brain tissues from AD donors and protein binding panels were used to determine [^{18}F]GTP1 binding characteristics. Stability was evaluated in vitro and in vivo in mice and rhesus monkey. In the clinic, whole-body imaging was performed to assess biodistribution and dosimetry. Dynamic [^{18}F]GTP1 brain imaging and input function measurement were performed on two separate days in 5 β-amyloid plaque positive (Aβ+) AD and 5 β-amyloid plaque negative (Aβ-) cognitive normal (CN) participants. Tracer kinetic modeling was applied and reproducibility was evaluated. SUVR was calculated and compared to [^{18}F]GTP1-specific binding parameters derived from the kinetic modeling. [^{18}F]GTP1 performance in a larger cross-sectional group of 60 Aβ+ AD participants and ten (Aβ- or Aβ+) CN was evaluated with images acquired 60 to 90 min post tracer administration.

Results [^{18}F]GTP1 exhibited high affinity and selectivity for tau pathology with no measurable binding to β-amyloid plaques or MAO-B in AD tissues, or binding to other tested proteins at an affinity predicted to impede image data interpretation. In human, [^{18}F]GTP1 exhibited favorable dosimetry and brain kinetics, and no evidence of defluorination. [^{18}F]GTP1-specific binding was observed in cortical regions of the brain predicted to contain tau pathology in AD and exhibited low (< 4%) test-retest variability. SUVR measured in the 60 to 90-min interval post injection correlated with tracer-specific binding (slope = 1.36, $r^2 = 0.98$). Furthermore, in a cross-sectional population, the degree of [^{18}F]GTP1-specific binding increased with AD severity and could differentiate diagnostic cohorts.

Conclusions [^{18}F]GTP1 is a promising PET probe for the study of tau pathology in AD.

This article is part of the Topical Collection on Translational Research

Sandra Sanabria Bohórquez and Jan Marik are co-first authors.

Electronic supplementary material The online version of this article (https://doi.org/10.1007/s00259-019-04399-0) contains supplementary material, which is available to authorized users.

✉ Robby M. Weimer
weimer.robby@gene.com

[1] Clinical Imaging Group, Genentech, Inc., 1 DNA Way, South San Francisco, CA 94080, USA

[2] Department of Biomedical Imaging, Genentech, Inc., 1 DNA Way, South San Francisco, CA 94080, USA

[3] Invicro LLC, 60 Temple St, Suite 8A, New Haven, CT 06510, USA

[4] XingImaging, LLC, 760 Chapel Street, New Haven, CT 06510, USA

[5] Department of Neuroscience, Genentech, Inc., 1 DNA Way, South San Francisco, CA 94080, USA

[6] Clinical Biostatistics, Genentech, Inc., 1 DNA Way, South San Francisco, CA 94080, USA

[7] Early Clinical Development, Genentech, Inc., 1 DNA Way, South San Francisco, CA 94080, USA

[8] Alector, Inc., 151 Oyster Point Blvd, South San Francisco, CA 94080, USA

Keywords Alzheimer's disease · Tau PET imaging · [^{18}F]GTP1 · Kinetic modeling

Introduction

Alzheimer's disease (AD) is a neurodegenerative disorder defined by the presence of extracellular β-amyloid plaques, consisting of aggregated Aβ peptide, and intracellular neurofibrillary tangles, comprised of aggregated hyperphosphorylated tau protein. The advent of pathology-specific PET tracers, such as β-amyloid plaque-specific tracers [^{11}C]PiB and [^{18}F]florbetapir, has revolutionized our understanding of AD pathophysiology. For example, β-amyloid plaques can be detected by PET imaging in individuals' years, even decades, prior to clinical symptom onset [1, 2].

The recent identification of first-generation tau-selective PET tracers, such as [^{18}F]AV-1451 (a.k.a. [^{18}F]T807, flortaucipir) [3], [^{18}F]T808 [4] and [^{11}C]PBB3 [5–7], is now beginning to enable the study of tau pathology in AD. While pivotal in demonstrating the feasibility of tau PET imaging, technical limitations have been reported for these first-generation tracers. For example, the initial clinical evaluation of [^{18}F]T808 revealed that the tracer exhibited a desirable brain kinetic profile and specific uptake in brain regions of AD patients consistent with the described distribution of tau pathology in disease [4]. However, [^{18}F]T808 also exhibited substantial metabolic instability resulting in apparent defluorination and [^{18}F]fluoride accumulation in bone [4]. Limitations of other first-generation tracers include suboptimal pharmacokinetics (e.g., low brain penetration, slow clearance), photo-instability, and binding to targets other than tau pathology, which has spurred the development and evaluation of second-generation tau PET tracers, such as [^{18}F]JNJ64349311 [8], [^{18}F]MK-6240 [9, 10], and [^{18}F]RO6958948 [11].

Isotopic substitution of hydrogen by deuterium has become the subject of research for active pharmaceutical agents (see, e.g., [12]). Isotopic substitution has also been applied to certain PET tracers containing ^{18}F as a radiolabel [12–14] in a manner that can reduce the formation of free [^{18}F]fluoride. We hypothesized that isotopic substitution of hydrogens on the carbon carrying ^{18}F of [^{18}F]T808 could reduce metabolism of the tracer in vivo, and thus mitigate the generation of [^{18}F]fluoride. Here we report the identification and preclinical and clinical evaluation of [^{18}F]GTP1 (Genentech Tau Probe 1) [15, 16], a tau-selective PET tracer with improved imaging properties.

Methods

Synthesis of radioligands

[^{18}F]T808 and [^{18}F]florbetapir for preclinical studies were synthesized at Genentech according to previously published protocols [4, 17]. [^{18}F]GTP1 for in vivo mice and in vitro studies was manufactured at Genentech [16]. The radiochemical purity of tracers was greater than 99% and specific activity was in the range 2590–4070 GBq/μmol. [^{18}F]GTP1 and [^{18}F]T808 for non-human primate studies and [^{18}F]GTP1 for clinical studies were synthesized at Invicro following previous published procedures [4, 16]. Quality control testing included strength (γ-assay), radiochemical purity and identity (UV and RadioHPLC), specific activity, pH, visual inspection, pyrogenicity, and sterility by compendial tests.

In vitro liver microsome assay

Human, rhesus and mice liver microsomes were obtained from BD Gentest (Bedford, MA, USA). Radioligands were dissolved in potassium phosphate (Kpi) buffer (100 mM) at a concentration of 18.5–22.2 MBq/ml. The reaction vessel was charged with mouse, rhesus, or human liver microsome suspension (12.5 μl, 20 mg/ml) followed by Kpi buffer (388 μl, 10 mM) and NADPH (50 μl, 10 mM), then incubated at 37 °C for 5–10 min. Radioligand (50 μl, 9.3–11.1 MBq) was added to the reaction vessel and the mixture was incubated at 37 °C. Aliquots (50 μl) of the reaction mixture were taken at 5, 15 and 45 min post addition of the tested compound, mixed with ice-cold acetonitrile (100 μl) and centrifuged. The supernatant was analyzed by RadioHPLC. The experiments were carried out in triplicate, with and without NADPH (VWR International; Randor, PA, USA) and testosterone (Sigma-Aldrich; Milwaukee, WI, USA) was used as positive control for microsomal activity (data not shown).

Autoradiography and competition binding assays

Frozen unfixed cortical tissues from AD donors, confirmed by neuropathological diagnosis using CERAD criteria, were obtained from Banner Sun Health Research Institute (Sun City, AZ, USA). The individual tissues were further evaluated by immunohistochemical staining for β-amyloid plaques and neurofibrillary tangles to confirm presence or absence of pathology in each sample (data not shown). The no-carrier-added [^{18}F]GTP1 was dissolved in PBS containing 5% DMSO and 5% ethanol at final concentration 1.5 MBq/ml (111–174 pg/ml). Then, 0.5 ml of stock solution was transferred to a microscope slide with 5-μm-thick freshly dried tissue section and incubated for 90 min at room temperature (RT). The slides were washed by dipping into the following chilled (4°C) solutions: PBS for 1 min, 70% ethanol 2 min, 30% ethanol 2 min and PBS 1 min. The samples were dried at RT for 30 min and exposed on a phosphorimager plate for 20 h. Autoradiography data was collected on a Typhoon FLA 9500 (GE Healthcare Bio-Sciences; Uppsala, Sweden)

phosphorimager using FujiFilm Imaging BAS-SR 2025 (Kanagawa, Japan) plates. The exposed plates were scanned at 25-μm resolution. For autoradiographic competition assays, increasing concentrations of L-deprenyl (0–10 μM), AV-1451 (0–0.5 μM) or GTP1 (0–1.0 μM) were added to the incubation solution and K_d and B_{max} were determined by non-linear fitting.

Preclinical imaging studies

All experiments were conducted in accordance with the United States Public Health Service's Policy on Humane Care and Use of Laboratory Animals. Study protocols were reviewed and approved by Institutional Animal Care and Use Committees. Preclinical dynamic PET studies in mice ($n = 6$) and in one rhesus monkey were performed to investigate [^{18}F]GTP1 and [^{18}F]T808 in vivo brain penetration, kinetics, and bone uptake. C57BL/6 mice were purchased from Harlan Laboratories (Livermore, CA, USA). Mouse imaging was performed on an Inveon PET/CT scanner (Siemens Medical Solutions USA Inc.) following a [^{18}F]GTP1 or [^{18}F]T808 intravenous dose of ~ 3.7 MBq. Rhesus monkey imaging was performed in a Focus 220 microPET camera following ~ 185 MBq doses of the radiotracers. Images were analyzed in PMOD 3.607 software (PMOD Technologies, Switzerland).

Human participants

Participants included here were enrolled in three clinical studies: a whole-body (WB) dosimetry study, a test retest study (TRTS), and a natural history study (NHS). Demographics and clinical characteristics are shown in Table 1. Significant differences in average age were not observed between the CN and AD cohorts for the TRTS and NHS ($p > 0.05$, Mann–Whitney U test). Detailed inclusion criteria can be found in the Supplementary Material. Written informed consent was obtained for all participants and/or their legally authorized representatives in accordance with federal and institutional guidelines. The study protocols were reviewed and approved by the New England Institutional Review Board (Needham, MA, USA).

Whole-body dosimetry study: Image acquisition and processing

WB imaging studies were performed on a Siemens HR+ PET camera. Individuals received a bolus intravenous administration of 339 ± 30 MBq of [^{18}F]GTP1 followed by a 10-ml saline flush. Starting with [^{18}F]GTP1 administration, a series of WB PET images (nine bed positions) were acquired over ~ 5.5 h in three scanning sessions (five WB passes, 2 × 1 min/bed and 3 × 2 min/bed; 2 WB passes, 2 × 4.5 min/bed; and 2 WB passes, 2 × 4.5 min/bed) with ~ 30 min breaks between them. A transmission scan was acquired prior to each imaging segment. PET images were corrected for attenuation, randoms, scatter, and isotope decay relative to the acquisition start time. Radioactivity urinary excretion was measured at three time points after each scanning session and up to 7 h post-injection. WB PET images were analyzed using PMOD 3.607 software (PMOD Technologies, Zurich, Switzerland) (see Supplementary Methods).

Brain studies: Image acquisition and processing

PET images were acquired on a Siemens HR+ or Siemens Biograph 6 PET-CT scanners (Table 2) and were reconstructed with an iterative reconstruction algorithm (OSEM four iterations, 16 subsets) and a post hoc 5-mm Gaussian filter. All [^{18}F]GTP1 PET studies were conducted in the same scanner for a given participant. A structural three-dimensional sagittal T1-weighted MR image (MP-RAGE or SPGR; 1 mm^2 in plane resolution, 1.0–1.2 mm slice thickness) was also acquired for all participants in a 1.5-T or 3-T MRI scanner using the manufacturer's recommended acquisition parameters. For the TRTS, the average interval between [^{18}F]GTP1 scans was 10 ± 6 (3–25, $n = 18$) days. Image processing and data analysis were performed using SPM12 and in-house developed analysis software in MATLAB (MathWorks Inc). Images were normalized to the standard MNI (Montreal Neurological Institute) space and regions of interest (ROIs) were defined for each participant using the automated anatomical labeling (AAL) brain atlas. The cerebellar cortex region was defined using a modified cerebellum SUIT template (http://www.diedrichsenlab.org/imaging/suit.htm) to include only the inferior cerebellum to avoid spillover from the surrounding temporal and occipital regions in AD participants (Supplementary Methods).

Blood sample processing

In the TRTS, 21 arterial samples (1.5 to 5 ml/sample) were withdrawn throughout the duration of the dynamic scans for measurement of the [^{18}F]GTP1 arterial input function (AIF). Additionally, two samples (~ 7 ml/sample) were drawn prior to [^{18}F]GTP1 injection for estimation of the parent free fraction (protein unbound) in plasma. Measurement of the radioactivity concentration in whole blood and plasma, [^{18}F]GTP1 plasma free fraction, [^{18}F]GTP1 plasma fraction and metabolite analysis were performed using standard methods (Supplementary Methods). Blood data were not available for the retest scan of one CN.

Kinetic modeling and calculation of SUVR

The [^{18}F]GTP1 AIF was obtained by multiplying the measured arterial plasma total activity and the corresponding

Table 1 Demographics and clinical characteristics

Study	Participants	*N* (female)	Age (years)	MMSE mean ± SD (range)	CDR score mean ± SD (range)	Florbetapir SUVR
Dosimetry	CN	6 (3)	38 ± 13	NA	NA	NA
Test-retest study[a]	CN Aβ-	5 (3)	59 ± 7 (51–67)	29 ± 1 (28–30)	0	1.00 ± 0.05
	AD	5 (3)	69 ± 10 (52–77)	22 ± 8 (10–27)	0.80 ± 0.67 (0.5–2)	1.38 ± 0.11
Natural history study (NCT02640092)[b]	CN Aβ-	2 (1)	52,71	28, 30	0	0.97, 1.07
	CN Aβ+	8 (5)	69 ± 3 (64–75)	29 ± 1 (28–30)	0	1.22 ± 0.18
	Prodromal AD	27 (14)	69 ± 8 (52–83)	28 ± 2 (24–30)	0.5	1.37 ± 0.15
	Mild AD	18 (10)	71 ± 6 (59–80)	25 ± 3 (22–30)	0.63 ± 0.23 (0.5–1)	1.40 ± 0.14
	Moderate AD	15 (7)	70 ± 7 (54–82)	18 ± 2 (16–21)	0.97 ± 0.34 (0.5–2)	1.41 ± 0.16

CN cognitive normal subjects, *Aβ−/+* β-amyloid plaque negative/positive by visual read; *MMSE* Mini-Mental State Examination, *CDR-SB* Clinical Dementia Rating, sum of boxes, *NA* not applicable; *florbetapir SUVR* calculated using the whole cerebellum

[a] Two participants in the Test-Retest Study (TRTS) subsequently enrolled in the Natural History Study (NHS)

[b] Eight AD participants underwent a repeat scan at visits 3 (five participants) or 4 (three participants) of the NHS including the two participants initially enrolled in the TRTS

plasma parent fraction determined by fitting the measured fraction to the bi-exponential function $ae^{-bt} + ce^{-dt}$ (a, b, c, $d \geq 0$). The maximum value of the parent fraction was set to 1 when calculating the AIF.

[^{18}F]GTP1 brain kinetics were described by applying a single-tissue (1T) or a two-tissue (2T) reversible compartmental models using the AIF [18]. The vascular contribution to the tissue TACs was included as an additional parameter in both models. The 1T and 2T models were compared using the Akaike Information Criteria (AIC) for measuring the trade-off between the goodness of fit and the number of model parameters. In addition, the [^{18}F]GTP1 total volume of distribution V_T was calculated using the AIF Logan graphical analysis (AIF-LGA) [19].

[^{18}F]GTP1-specific binding, or BP_{ND}, in cortical target regions was calculated using as $(V_T–V_{ND})/V_{ND}$ and the distribution volume ratio (DVR) was calculated as V_T/V_{ND} or $BP_{ND} + 1$, were the non-displaceable distribution volume V_{ND} was estimated based on the total distribution volume V_T within the cerebellar cortex since this brain region is not predicted to contain tau pathology in AD [20, 21]. The cerebellum cortex was also used as an indirect input to calculate DVRs using a simplified reference tissue model (SRTM) [22], and as reference region for calculating the standardized uptake value ratios (SUVR). The AIF and cerebellum curves were interpolated for obtaining the timepoints needed for applying AIF-LGA and SRTM, respectively (see Supplementary Material). The test-retest variability was calculated as 100 × (retest-test)/((test+retest)/2) for DVR and SUVR measurements.

Cross-sectional evaluation of [^{18}F]GTP1

Group differences in [^{18}F]GTP1-specific binding between CN and AD cohorts were assessed by calculating Hedge's effect size (ES) with 95% confidence interval (CI) [23], statistical significance was assessed by Mann–Whitney *U* tests. Comparisons were performed in the following composite ROIs: a whole cortical gray matter (GM) obtained from the gray matter MRI segmentation, in vivo Braak ROIs [24] (excluding basal ganglia and thalamus regions), and a temporal meta-ROI proposed to capture early disease-related tau pathology deposition [25]. The Braak ROIs and the temporal meta-ROI were created using the Hammersmith atlas (http://brain-development.org/brain-atlases/adult-brain-atlases/adult-brain-maximum-probability-map-hammers-mith-atlas-n30r83-in-mni-space) because of the more detailed parcellation of the temporal lobe regions (see Supplementary Materials). For the purposes of these analyses, participants were defined as Aβ+ if their florbetapir SUVR was above 1.10 in a composite cortical ROI using the whole cerebellum as reference [26].

Table 2 Brain imaging protocol

Studies	Participants	Injected dose MBq ± SD (range)	Injected mass μg ± SD (range)	Arterial blood sampling	Acquisition segments (number of frames × duration)	PET scanner
TRTS	CN, $n = 5$ AD, $n = 5$	333 ± 24 (267–249) 338 ± 27 (265–354)	0.19 ± 0.10 (0.09–0.43) 0.23 ± 0.16 (0.09–0.43)	Yes Yes	0–30 min (6 × 30 s, 4 × 1 min, 4 × 2 min, 3 × 5 min) 60–120 min (12 × 5 min) 150–180 min (6 × 5 min) A transmission scan was acquired prior to each imaging segment	HR+
NHS	AD with a reproducibility scan, $n = 8$	352 ± 7 (331–359)	0.93 ± 1.07 (0.07–2.79)	No	60–90 min (6 × 5 min)	PET-CT ($n = 7$) HR+ ($n = 1$)
	CN and AD ($n = 64$)	343 ± 33 (188–365)	1.33 ± 0.96 (0.04–5.53)	No		PET-CT ($n = 63$) HR+ ($n = 1$)

Results

Identification and in vitro characterization of [^{18}F] GTP1

To compare catabolism of the tracers [^{18}F]T808 and [^{18}F]GTP1, we incubated each tracer in liver microsome suspension from mouse, rhesus, or human and assessed the formation of free [^{18}F]fluoride in the presence or absence of NADPH (Fig. 1b). In mouse, rhesus, or human-derived liver microsome suspensions, [^{18}F]T808 was metabolized rapidly to two polar metabolites and [^{18}F]fluoride. Nearly half of the radioactivity (mouse, 50.1 ± 12.9%; rhesus, 46.1 ± 1.0%; human, 36.7 ± 2.7%) at the end of study representing [^{18}F]fluoride. In contrast, incubation of [^{18}F]GTP1 in mouse or rhesus derived liver microsomes produced significantly less [^{18}F]fluoride (mouse, 13.8 ± 2.4%, $p = 0.035$; rhesus, 15.4 ± 1.3%, $p = 8.4 \times 10^{-6}$). In addition, no [^{18}F]fluoride was detected when [^{18}F]GTP1 was incubated in human liver microsome suspensions ($p = 0.002$), and the [^{18}F]GTP1 parent fraction at the end of the assay was significantly higher than that of [^{18}F]T808 (67.1 ± 6.3 and 35.7 ± 0.9%, respectively, $p = 0.012$). In all cases, the formation of metabolites was NADPH dependent, indicating the involvement of the cytochrome P450 complex in tracer metabolism. These data suggests that [^{18}F]GTP1 has higher metabolic stability than [^{18}F]T808 in vitro, and predicts that [^{18}F]GTP1 is unlikely to be metabolized to generate [^{18}F]fluoride in human subjects, thus potentially mitigating the bone uptake observed with [^{18}F]T808. The two oxidative metabolites observed in the microsomal stability studies are more polar than the parent [^{18}F]GTP1 and they are unlikely able to cross the blood–brain barrier and interfere with the signal originating from [^{18}F]GTP1.

We next evaluated if [^{18}F]GTP1 retained binding selectivity to tau pathology in Alzheimer's disease. In a series of tissue binding autoradiography studies using cortical tissues from AD donors, [^{18}F]GTP1 selectively bound to tissues confirmed to contain tau pathology but not to tissues containing β-amyloid plaques alone (Fig. 1c). Scatchard analysis of the bound and unbound fraction as a function of concentration showed [^{18}F]GTP1 binds to tau pathology with high affinity, K_d of 10.8 ± 1.1 nM and B_{max}/K_d ratio values between 12 and 100 (Table 3). Furthermore, the tau-selective radioligand Flortaucipir (a.k.a. [^{18}F]AV1451, [^{18}F]T807) competed with [^{18}F]GTP1 in tau-positive tissues with a maximum competitive binding at 1 μM [^{18}F]AV-1451 of ~ 82%, and an estimated IC_{50} of 22 nM (Supplementary Fig. 1).

Due to recent reports of off-target binding by first-generation tau PET tracers (e.g., binding of [^{18}F]THK5351 to MAO-B) [27], the binding specificity of [^{18}F]GTP1 was further evaluated. The binding affinity of [^{18}F]GTP1 for MAO-B was assessed using the MAO-B ligand L-deprenyl

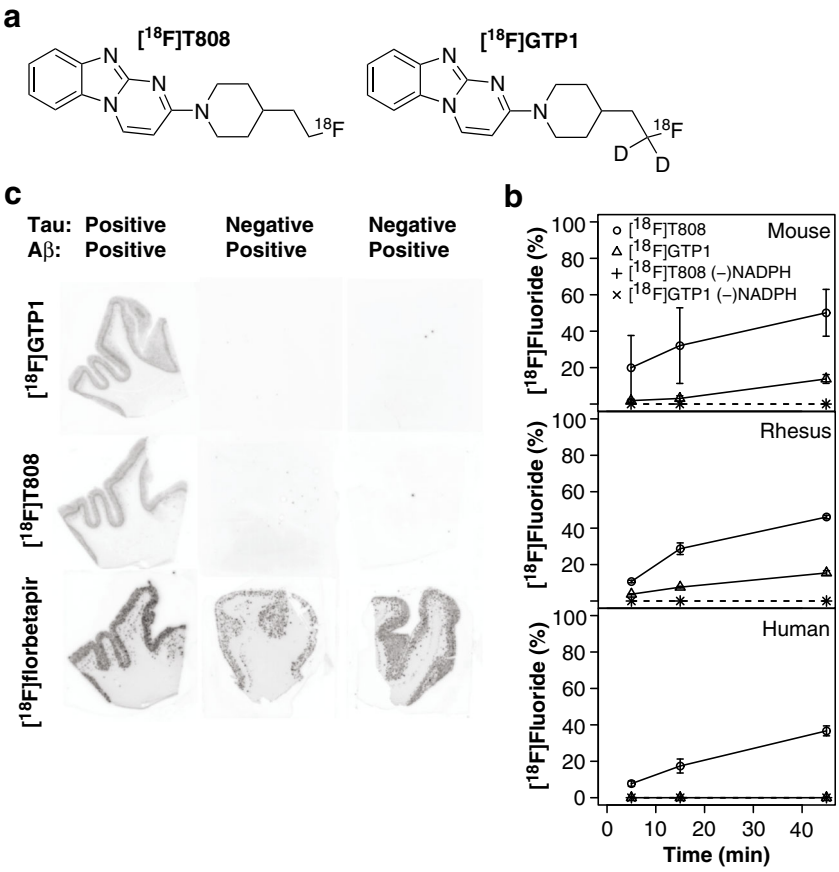

Fig. 1 Chemical structures of [^{18}F]T808 and [^{18}F]GTP1 (**a**). Stability of [^{18}F]GTP1 and [^{18}F]T808 in liver microsomes isolated from indicated species presented as a fraction of [^{18}F]fluoride measured by RadioHPLC at 0–45 min (**b**). Binding profiles of [^{18}F]GTP1, [^{18}F]T808, and [^{18}F]florbetapir to adjacent sections of tau-positive or tau-negative cortical tissues from AD patients detected by autoradiography (**c**)

in competitive binding autoradiography assays. Increasing concentrations of L-deprenyl up to 10 μM did not reduce [^{18}F]GTP1 binding to tau-positive AD cortical tissues (Supplementary Fig. 1), suggesting that [^{18}F]GTP1 does not bind to MAO-B. Additionally, [^{18}F]GTP1 binding was not detected to brain expressed proteins at an affinity lower than 1 μM in the in vitro binding panels (CEREP) and follow-up functional assays performed with targets showing greater than 75% inhibition at 10 μM, supporting the notion that [^{18}F]GTP1 represents a tau-selective radioligand (Supplementary Tables 1–3).

Preclinical imaging

In mice and rhesus, [^{18}F]GTP1 exhibited rapid brain penetration followed by fast clearance throughout the brain with no apparent specific binding (Supplementary Fig. 2 and 3). In both species, radioactivity uptake was observed in the skull, likely due to low levels of defluorination of the compound in vivo. However, the level of skull uptake for [^{18}F]GTP1 was significantly lower than that observed for [^{18}F]T808 in mice (31.2 ± 4.8 vs. 14.3 ± 1.7 %ID/g at 30–45 min, $p = 1.19 \times 10^{-4}$) and lower in rhesus (1.8 vs. 0.5 SUV at 240 min), consistent with the predicted increased metabolic stability of [^{18}F]GTP1 from the in vitro liver microsome stability assays.

Table 3 Characteristics of autoradiographic binding assay using [^{18}F]GTP1 and human tissues

Sample ID	Kd (nM)	Bmax (nM)	Bmax/Kd
775	11.8	547	46
773	9.7	972	100
781	10.8	130	12

Clinical imaging safety summary

[^{18}F]GTP1 and the study procedures were well tolerated. All reported adverse events (AEs) were non-serious and mild. The only AEs reported in at least two participants were non-serious mild ecchymosis ($n = 5$) and non-serious mild hypertension ($n = 2$). No clinically significant change in vital signs or the results of laboratory studies or electrocardiograms was observed.

Whole-body dosimetry

Dosimetry estimates were calculated in the following: brain, liver, gallbladder, intestines, urinary bladder (UB), heart,

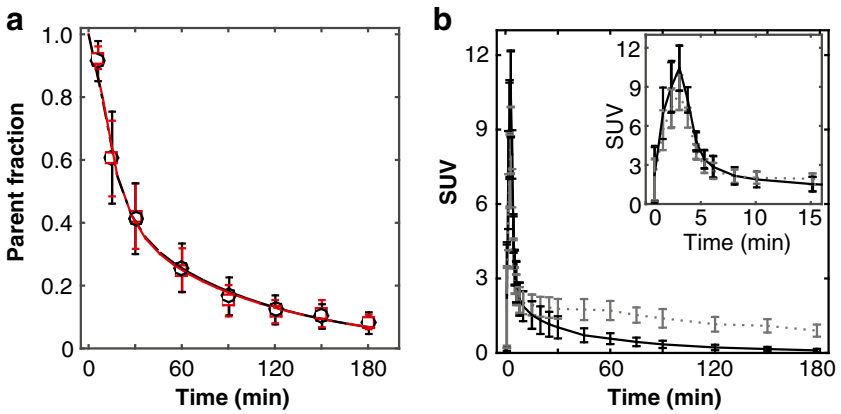

Fig. 2 Measured [^{18}F]GTP1 parent fraction in arterial plasma (**a**). *Black* and *red symbols* represent the average parent fraction in CN (five participants, nine scans) and AD (five participants, ten scans), respectively. *Error bars* correspond to the standard deviation. The *solid red* and *dashed black lines* correspond to the bi-exponential fitted curve to the CN and AD, respectively. Average (mean ± SD) [^{18}F]GTP1 plasma concentration, *solid line*, and average radioactivity concentration in blood, *dotted line* (**b**)

kidneys, spleen, and lungs (Supplementary Fig. 4 and 5, Supplementary Tables 4 and 5). The radiotracer was eliminated via both hepatobiliary and urinary pathways, with a maximum of ~ 25–40% injected dose (ID) in the liver and up to ~ 10 %ID in the intestine. The total cumulative radioactivity present in urine was measured to be ~ 37 ± 6 %ID. No radioactivity accumulation was observed in bone.

The target organ with highest exposure was the urinary bladder (UB) in females (1.75×10^{-1} mSv/MBq) and gallbladder in males (1.18×10^{-1} mSv/MBq). The gallbladder was

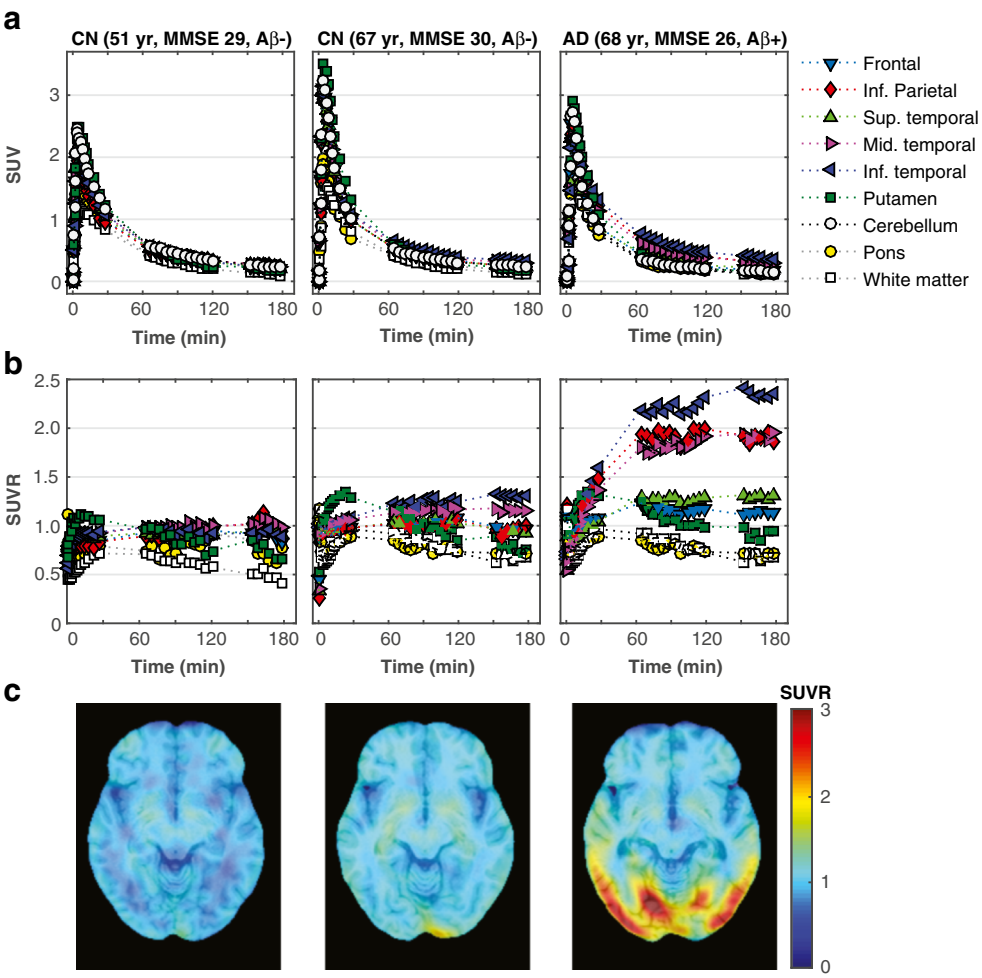

Fig. 3 Representative [^{18}F]GTP1 time activity curves (**a**), their corresponding SUVR curves calculated using cerebellum as reference region (**b**), and SUVR imagines (60–90 min) for two CN and one AD participant (**c**). Aβ −/+: β-amyloid plaque negative/positive

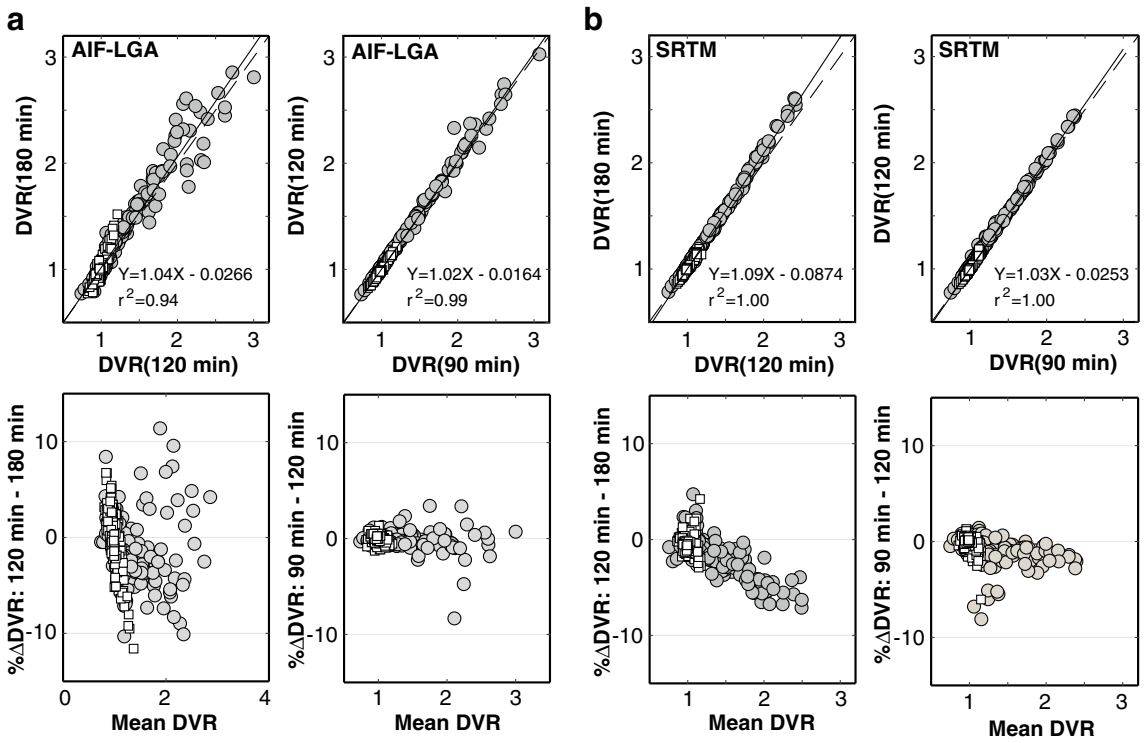

Fig. 4 Time stability of [^{18}F]GTP1-specific binding measurements using cerebellum cortex as reference region derived from AIF-LGA (**a**), or SRTM (**b**). Each *point* corresponds to a region in the AAL template in a given participant. CN, *open squares*; AD, *filled circles*; *solid line*, linear regression; *dashed lines*, identity line

identified as the critical organ for both males (1.65×10^{-1} mSv/MBq) and females (1.17×10^{-1} mSv/MBq) when a 2-h UB voiding model was employed. The effective dose (ED) was estimated to be $3.48 \times 10^{-2} \pm 2.42 \times 10^{-3}$ mSv/MBq (adult female) and $2.66 \times 10^{-2} \pm 9.81 \times 10^{-4}$ mSv/MBq (adult male) with no UB voiding, and $3.24 \times 10^{-2} \pm 2.93 \times 10^{-3}$ mSv/MBq (adult female) and $2.49 \times 10^{-2} \pm 1.30 \times 10^{-3}$ mSv/MBq (adult male) with 2-h UB voiding interval. Average ED values (all participants) were $3.07 \times 10^{-2} \pm 4.78 \times 10^{-3}$ with no UB voiding, and $2.86 \times 10^{-2} \pm 4.56 \times 10^{-3}$ mSv/MBq with 2-h UB voiding interval. These results are similar those of other ^{18}F-based radiotracers.

Plasma kinetics

On average, the [^{18}F]GTP1 fraction in plasma across the CN and AD populations was similar, with about 15% of the intact parent compound remaining at 90 min post injection (Fig. 2). The [^{18}F]GTP1 non-protein-bound fraction in plasma was low, $1.1 \pm 0.4\%$ ($n = 19$), and similar between the two groups (1.2 and 1.1% in AD and CN, respectively). All metabolites identified after RadioHPLC separation were more polar than the parent compound (Supplementary Fig. 6).

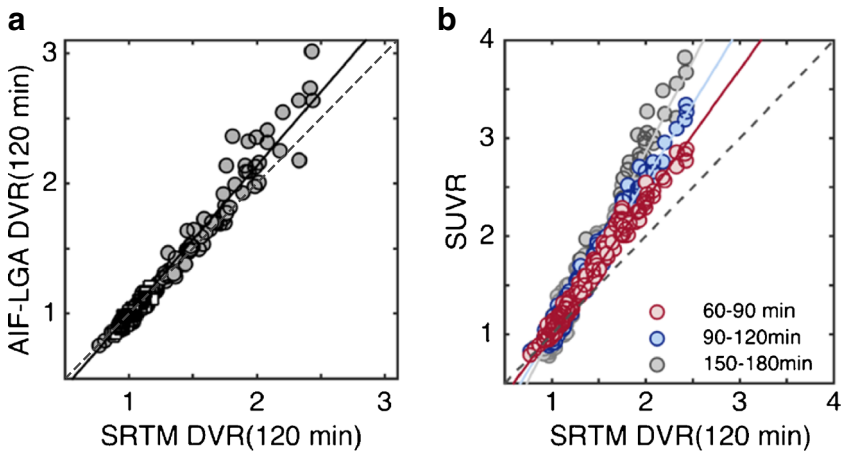

Fig. 5 Relationship between [^{18}F]GTP1 AIF-LGA DVR and SRTM DVR values (**a**) and SUVR and SRTM DVR values (**b**). Each *point* corresponds to a region in the AAL template in a given participant. For **a**; CN, *open squares*; AD, *filled circles*. For **b**; *gray circles*, SUVR(150–180 min); *blue circles*, SUVR(90–120 min; *red circles*, SUVR(60–90 min). *Solid lines*, linear regressions ($r^2 \geq 0.95$)

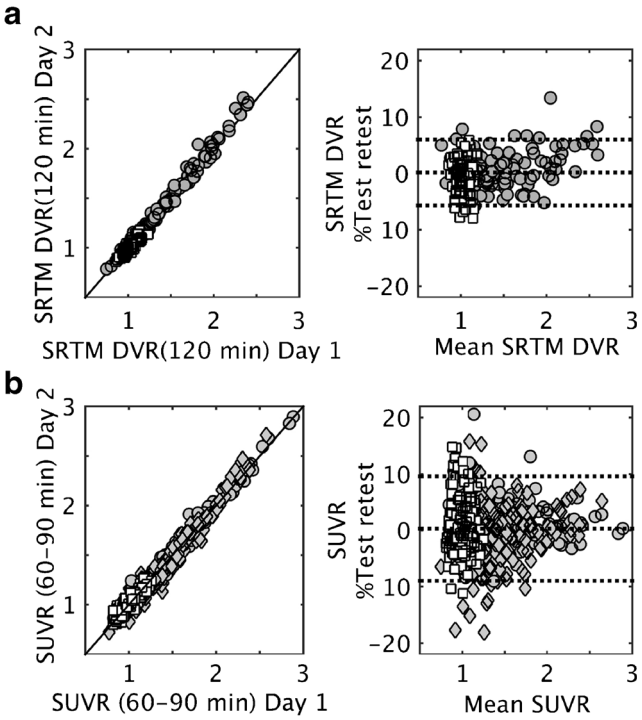

Fig. 6 Scatter and Bland–Altman plots comparing test and retest SRTM DVR values ($n = 10$) (**a**) and SUVR values ($n = 18$, two participants with two sets of test and retest images) (**b**). Each *point* corresponds to a region in the AAL template in a given participant. AD, *filled circles* (TRTS, $n = 5$), *filled diamonds* (NHS, $n = 8$); CN, *open squares* ($n = 5$); *solid line*, linear regression (both $r^2 = 0.99$); *dotted line*, mean and mean ± 2 standard deviations

Brain kinetics

In CNs, the uptake and clearance kinetics of [^{18}F]GTP1 were similar between cortical regions and cerebellum (Fig. 3). In AD participants, a higher uptake level was typically observed in cortical regions starting as early as ~ 20 min after tracer administration, reaching secular equilibrium ~ 60 to 90 min post injection. No radioactivity accumulation was observed in the skull. White matter and pons exhibited the lowest uptake level, with SUVR values decreasing with time.

In a subset of CN and AD participants, SUVR images from the 60 to 90-min interval revealed a slightly elevated signal in the putamen and globus pallidus. The results from the kinetic modeling (see Supplementary Material) suggested that the use of the cerebellum as a reference for these specific target regions underestimates the non-displaceable component of the measured signal. Therefore, the SUVR values in the putamen and globus pallidus, calculated using the cerebellum as a reference, may not convey reliable information regarding tracer-specific binding irrespective of source (i.e., on- or off-target) (Supplementary Fig. 7). Due to their location and the relatively low SUVR values, signal in the putamen and globus pallidus should not interfere with the analysis of tracer-specific binding in the cortical areas of interest in AD.

Kinetic modeling

The [^{18}F]GTP1 kinetics in cerebellum and in cortical regions with low tracer accumulation were best described using a one-tissue compartment (1T) model, whereas in regions with higher tracer accumulation a two-tissue compartment (2T) model was more appropriate (Supplementary Fig. 8). The average K_1 across all brain regions, calculated using 120 min of scan data in all participants, was 0.10 ± 0.03 ml.cm^{-3}.min^{-1}. Regional values are shown in Supplementary Table 6. Assuming a standard brain blood flow rate of 0.6 ml.cm^{-3}.min^{-1}, the first pass extraction is estimated to be $17 \pm 5\%$.

[^{18}F]GTP1 V_T measures across all cortical brain regions were calculated using AIF-LGA because this method does not require assumptions about the number of tissue compartments (see Supplementary Fig. 9 with a typical AIF-LGA plot). AIF-LGA DVR values calculated using variable scan lengths were linearly correlated, $r^2 > 0.94$ (Fig. 4a). The lower count rate in the 150 to 180-min time interval relative to the earlier imaging segments resulted in an increase in noise in the plasma curves, which affected V_T and DVR estimates. The relationships between the AIF-LGA DVR(180 min) and the AIF-LGA DVR(120 min) or AIF-LGA DVR(90 min) were similar with most values within ± 5% when using the shorter scan lengths.

When using a simplified reference tissue model (SRTM) to derive DVR estimates, R_1 and DVR values within a cortical region were similar and accurately estimated (based on unique solution and small parameter estimation uncertainties) whether using a region-specific k_2' value or a common k_2' estimated for each scan by simultaneously fitting all cortical regions [28]. Therefore, we utilized the scan-specific k_2' to estimate SRTM DVR (Fig. 4b). SRTM DVR(120 min) values were slightly underestimated (≤ 8%) relative to DVR(180 min) values. The SRTM DVR(90 min) values were similar to those calculated for DVR(120 min) ($r^2 = 1.00$).

Comparison of AIF-LGA DVR and SRTM DVR values demonstrate a linear relationship between the two methods for estimating specific binding (AIF-LGA DVR = 1.14 SRTM DVR(120 min) - 0.136; $r^2 = 0.97$) (Fig. 5a), supporting the use of SRTM as an alternative approach to performing dynamic acquisitions and blood measurements for quantification. Furthermore, SRTM DVR(120 min) was also linearly correlated ($r^2 \geq 0.95$) with SUVR estimates calculated using different time intervals (Fig. 5b). These findings suggest the [^{18}F]GTP1-specific binding in cortex can be reliably estimated using various scan durations, thus offering flexible options for clinical imaging protocols.

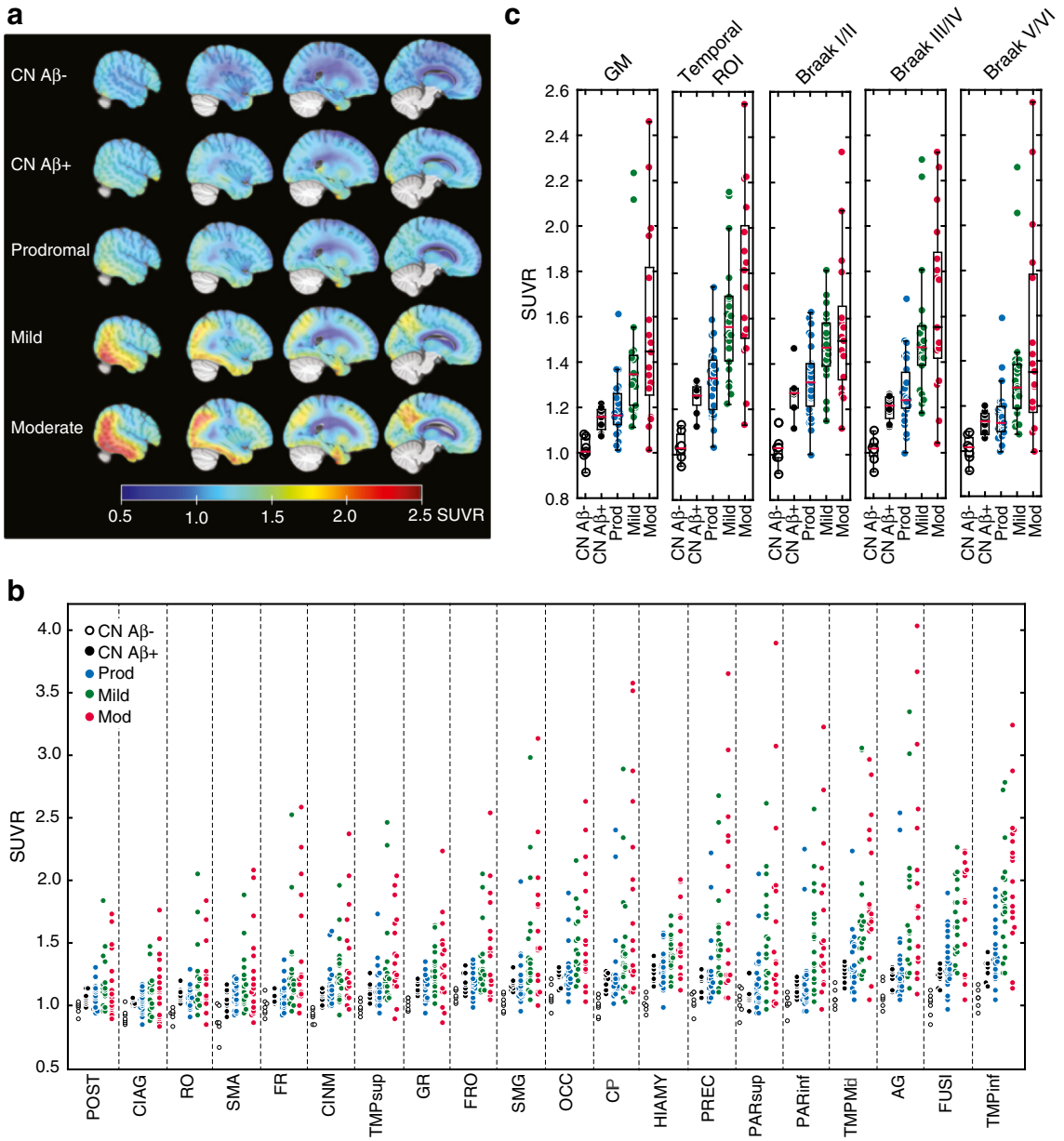

Fig. 7 Average [^{18}F]GTP1 SUVR images across participants per cohort (**a**). Regional boxplots of SUVR values (average in the left and right hemispheres) by clinical cohort. Regions are organized in ascending order based on the mean SUVR values in the mild and moderate AD subjects (**b**). Box plots of [^{18}F]GTP1 SUVR(60–90 min) values by clinical cohort calculated within the whole gray matter, the temporal-meta or the in vivo Braak ROIs (**c**). CN: cognitive normal subjects; Aβ−/+: β-amyloid plaque negative/positive; Prod., prodromal AD; Mild, mild AD; Mod, moderate AD. AAL ROIS: FR: Frontal cortex (excluding orbital regions), FRO: Frontal cortex, orbital regions; RO: Rolandic operculum; SMA: Supplementary motor area; GR: Gyrus rectus; CIAG: Cingulate gyrus, anterior part; CINM: Cingulate gyrus, mid part; CIP: Cingulate gyurs, posterior part; HIAMY: Hippocampus, Parahippocampus, Amygdala; OCC: Occipital cortex; FUSI: Fusiform gyrus; POST: Postcentral gyrus; PARsup: Superior parietal gyrus; PARinf: Inferior parietal gyrus; SMG: Supramarginal gyrus; AG: Angular gyrus; PREC: Precuneus; TMPsup: Superior temporal cortex; TMPmid: Mid temporal cortex; TMPinf: Inferior temporal cortex

Test re-test performance

The average absolute test-retest variability of SRTM DVR(120 min) was 2.24 and 95% of the changes were below 6% ($n = 10$, 38 ROIs per participant) (Fig. 6a). In these same participants and regions, the test-retest variability of SUVR calculated using the 60–90 min, 90–120 min, and 150–180 min time intervals were 3.73% (95%ile = 9.44%), 5.13% (95%ile = 14.22%) and 5.21% (95%ile = 12.79%), respectively, consistent with larger noise level due to lower counts statistics at later time intervals. Eight additional pairs of scans were acquired as part of the NHS with the acquisition time window of 60–90 min post injection. In this larger data set ($n = 18$), the average absolute SUVR test-retest variability was

3.51%, 95%ile = 9.10% (Fig. 6b). The largest variability values were observed for the smaller and less avid ROIs.

Cross-sectional evaluation of [^{18}F]GTP1 in Alzheimer's disease

In a cross-sectional cohort of CN ($n = 15$) and AD ($n = 65$) participants spanning prodromal to moderate disease, the distribution of [^{18}F]GTP1 binding as a function of disease severity (Fig. 7a, b), and was consistent with the described Braak staging of AD tau pathology [24]. SUVR values in the Braak I/II-related regions were elevated across all AD cohorts, while SUVR values in the Braak V/VI-related regions were elevated only in the mild and moderate cohorts (Fig. 7c). Furthermore, SUVR values calculated using either a whole cortical gray matter (GM) or a temporal meta-ROI differentiated between CN Aβ- and Aβ+ cohorts, as well as the individual AD cohorts (Fig. 7c, Supplementary Table 7), and found to correlate with cognition [29].

Discussion

In this work, we describe the identification, binding specificity, preclinical PK and clinical performance of [^{18}F]GTP1 as a tau PET tracer for AD. In tissue and in in vitro binding studies, [^{18}F]GTP1 bound to tau pathology with low nanomolar affinity, excellent selectivity over β-amyloid plaque, and no apparent off-target binding, in particular to MAO-B. The ability of [^{18}F]GTP1 to bind other forms of tau pathology present in non-AD tauopathies, for example filaments of 3-repeat tau present in Pick's disease, remains unexplored. In preclinical imaging studies, [^{18}F]GTP1 exhibited rapid brain uptake and clearance, and in clinical imaging studies [^{18}F]GTP1 exhibited properties supportive of its use as a tau PET tracer in AD.

[^{18}F]GTP1 kinetic modeling showed that the DVR values obtained using SRTM and AIF-LGA approaches were highly correlated. The regression slope between the two methods was close to unity with a small intercept value, indicating that the SRTM method can be as sensitive as AIF-LGA to measure [^{18}F]GTP1 DVR in cortical regions across the range of observed values in CN and AD participants. The DVR time stability suggests that [^{18}F]GTP1 kinetics can be well described using 90 or 120-min scan durations; the suitability of shorter duration scans was not fully investigated in this work.

In multi-site clinical studies, dynamic acquisitions may not be practical. Therefore, it is desirable to simplify the acquisition protocol and reduce the imaging time. Under these imaging conditions, SUVR is the preferred method of quantification. The tight linear relationship between SUVR in the 60–90 min, 90–120 min, or 150–180 min and SRTM DVR(120 min) suggests any of these time intervals could be used to estimate [^{18}F]GTP1-specific binding. A simplified imaging procedure that acquires data from 60 to 90 min post tracer administrations reduces the level of noise in the PET data and provides a robust estimate of [^{18}F]GTP1-specific binding with excellent test-retest reproducibility. Furthermore, given the favorable [^{18}F]GTP1 radiation profile, repeated imaging of the same participant in multi-site settings would be feasible.

In a cross-sectional cohort spanning prodromal to moderate AD, [^{18}F]GTP1 SUVR measures displayed a large dynamic range. In general, SUVR values increased with disease severity and differentiated between AD and CN cohorts and between brain regions predicted to contain high versus low tau burden, supporting the use of [^{18}F]GTP1 PET imaging as a biomarker of tau pathology in AD. When considered in the context of the observed low test-retest variability in SUVR measures (~ 4%), longitudinal [^{18}F]GTP1 PET imaging may provide a sensitive means for detecting tau pathology progression in disease and warrants further investigation.

To date, preclinical and clinical data have been published for a subset of candidate tau PET tracers; for a recent review see [30]. In comparison, [^{18}F]GTP1 complements and extends this library of tau PET tracer. Here we show that on tissue samples from AD subjects [^{18}F]GTP1 competes away binding of [^{18}F]AV1451, similar to published studies using [^{18}F]T808 [8, 9], [^{18}F]MK6420 [9] and [^{18}F]RO948 [31], therefore these tracers likely share a common binding site on neurofibrillary tau pathology in AD. The in vivo kinetics of [^{18}F]GTP1 observed in our studies, both preclinically and clinically, suggests that [^{18}F]GTP1 has a favorable PK profile that enables imaging in an time frame earlier than flortaucipir [32, 33], and [^{18}F]MK6420 [10]. However, further studies, including head-to-head comparisons, will be required to better understand comparability of these tracers.

Conclusions

[^{18}F]GTP1 exhibits high affinity and selectivity for tau pathology in AD. The tracer has good brain penetration and rapid washout, excellent test-retest reproducibility, and favorable radiation dosimetry profile. SUVR measured in the 60 to 90-min interval following administration is a robust surrogate of [^{18}F]GTP1-specific binding to tau. [^{18}F]GTP1 is a promising PET probe for the study of tau pathology in AD.

Acknowledgements The authors would like to thank Alex de Crespigny, Flavia Brunstein, Edward Teng, Kristin Wildsmith, Corinne Foo-Atkins, Reina Fuji, Gautham Rao, Michael Keeley, and Beth Blankemeier for their support and contribution to this work.

Compliance with ethical standards

Research involving human participants and/or animals.

Informed consent.

Conflict of interest All authors are paid employees of either Genentech Inc., or Invicro LLC and all work was funded by Genentech Inc.

Ethical approval All procedures performed in studies involving human participants were in accordance with the ethical standards of the institutional and/or national research committee and with the 1964 Helsinki Declaration and its later amendments or comparable ethical standards.

All applicable international, national, and/or institutional guidelines for the care and use of animals were followed.

References

1. Jack CR Jr, Wiste HJ, Vemuri P, Weigand SD, Senjem ML, Zeng G, et al. Brain beta-amyloid measures and magnetic resonance imaging atrophy both predict time-to-progression from mild cognitive impairment to Alzheimer's disease. Brain. 2010;133(11):3336–48. https://doi.org/10.1093/brain/awq277.
2. Bateman RJ, Xiong C, Benzinger TL, Fagan AM, Goate A, Fox NC, et al. Clinical and biomarker changes in dominantly inherited Alzheimer's disease. N Engl J Med. 2012;367(9):795–804. https://doi.org/10.1056/NEJMoa1202753.
3. Chien DT, Bahri S, Szardenings AK, Walsh JC, Mu F, Su MY, et al. Early clinical PET imaging results with the novel PHF-tau radioligand [F-18]-T807. Journal of Alzheimer's disease: JAD. 2013;34(2):457–68. https://doi.org/10.3233/JAD-122059.
4. Chien DT, Szardenings AK, Bahri S, Walsh JC, Mu F, Xia C, et al. Early clinical PET imaging results with the novel PHF-tau radioligand [F18]-T808. Journal of Alzheimer's disease: JAD. 2014;38(1):171–84. https://doi.org/10.3233/JAD-130098.
5. Maruyama M, Shimada H, Suhara T, Shinotoh H, Ji B, Maeda J, et al. Imaging of tau pathology in a tauopathy mouse model and in Alzheimer patients compared to normal controls. Neuron. 2013;79(6):1094–108. https://doi.org/10.1016/j.neuron.2013.07.037.
6. Kimura Y, Endo H, Ichise M, Shimada H, Seki C, Ikoma Y, et al. A new method to quantify tau pathologies with (11)C-PBB3 PET using reference tissue voxels extracted from brain cortical gray matter. EJNMMI Res. 2016;6(1):24. https://doi.org/10.1186/s13550-016-0182-y.
7. Kimura Y, Ichise M, Ito H, Shimada H, Ikoma Y, Seki C, et al. PET quantification of tau pathology in human brain with 11C-PBB3. J Nucl Med. 2015;56(9):1359–65. https://doi.org/10.2967/jnumed.115.160127.
8. Declercq L, Rombouts F, Koole M, Fierens K, Marien J, Langlois X, et al. Preclinical evaluation of (18)F-JNJ64349311, a novel PET tracer for tau imaging. J Nucl Med. 2017;58(6):975–81. https://doi.org/10.2967/jnumed.116.185199.
9. Hostetler ED, Walji AM, Zeng Z, Miller P, Bennacef I, Salinas C, et al. Preclinical characterization of 18F-MK-6240, a promising PET tracer for in vivo quantification of human neurofibrillary tangles. J Nucl Med. 2016;57(10):1599–606. https://doi.org/10.2967/jnumed.115.171678.
10. Pascoal TA, Shin M, Kang MS, Chamoun M, Chartrand D, Mathotaarachchi S, et al. In vivo quantification of neurofibrillary tangles with [18F]MK-6240. Alzheimers Res Ther. 2018;10(1):74. https://doi.org/10.1186/s13195-018-0402-y.
11. Wong DF, Comley R, Kuwabara H, Rosenberg PB, Resnick SM, Ostrowitzki S, et al. First in-human PET study of 3 novel tau radiopharmaceuticals: [(11)C]RO6924963, [(11)C]RO6931643, and [(18)F]RO6958948. J Nucl Med. 2018. https://doi.org/10.2967/jnumed.118.209916.
12. Gant TG. Using deuterium in drug discovery: leaving the label in the drug. J Med Chem. 2013. https://doi.org/10.1021/jm4007998.
13. Jahan M, Eriksson O, Johnstrom P, Korsgren O, Sundin A, Johansson L, et al. Decreased defluorination using the novel beta-cell imaging agent [18F]FE-DTBZ-d4 in pigs examined by PET. EJNMMI Res. 2011;1(1):33.
14. Schou M, Halldin C, Sovago J, Pike VW, Hall H, Gulyas B, et al. PET evaluation of novel radiofluorinated reboxetine analogs as norepinephrine transporter probes in the monkey brain. Synapse. 2004;53(2):57–67. https://doi.org/10.1002/syn.20031.
15. Marik J, Tinianow JN, Ogasawara A, Liu N, Williams SP, Lyssikatos JP, et al. [18F]GTP1 - A tau-specific tracer for imaging taupathology in AD. 10th Human Amyloid Imaging; January 13–15, 2016; Miami, FL 2016. p. 49 (PE32).
16. Marik J, Lyssikatos JP, Williams SP, inventors; US Patent No. 10, 076,581. Deuterated compounds and uses thereof. 2018 Sep. 18.
17. Choi SR, Golding G, Zhuang Z, Zhang W, Lim N, Hefti F, et al. Preclinical properties of 18F-AV-45: a PET agent for Abeta plaques in the brain. J Nucl Med. 2009;50(11):1887–94. https://doi.org/10.2967/jnumed.109.065284.
18. Innis RB, Cunningham VJ, Delforge J, Fujita M, Gjedde A, Gunn RN, et al. Consensus nomenclature for in vivo imaging of reversibly binding radioligands. J Cereb Blood Flow Metab. 2007;27(9):1533–9. https://doi.org/10.1038/sj.jcbfm.9600493.
19. Logan J. Graphical analysis of PET data applied to reversible and irreversible tracers. Nucl Med Biol. 2000;27(7):661–70.
20. Braak H, Braak E. Neuropathological stageing of Alzheimer-related changes. Acta Neuropathol. 1991;82(4):239–59.
21. Marquie M, Normandin MD, Vanderburg CR, Costantino IM, Bien EA, Rycyna LG, et al. Validating novel tau positron emission tomography tracer [F-18]-AV-1451 (T807) on postmortem brain tissue. Ann Neurol. 2015;78(5):787–800. https://doi.org/10.1002/ana.24517.
22. Lammertsma AA, Hume SP. Simplified reference tissue model for PET receptor studies. NeuroImage. 1996;4(3 Pt 1):153–8. https://doi.org/10.1006/nimg.1996.0066.
23. Hedges LV, Shymansky JA, Woodworth G. A practical guide to modern methods of meta-analysis. Washington, DC: National Science Teachers Association; 1989.
24. Scholl M, Lockhart SN, Schonhaut DR, O'Neil JP, Janabi M, Ossenkoppele R, et al. PET imaging of tau deposition in the aging human brain. Neuron. 2016;89(5):971–82. https://doi.org/10.1016/j.neuron.2016.01.028.
25. Jack CR Jr, Wiste HJ, Weigand SD, Therneau TM, Lowe VJ, Knopman DS, et al. Defining imaging biomarker cut points for brain aging and Alzheimer's disease. Alzheimers Dement. 2017;13(3):205–16. https://doi.org/10.1016/j.jalz.2016.08.005.
26. Landau SM, Breault C, Joshi AD, Pontecorvo M, Mathis CA, Jagust WJ, et al. Amyloid-beta imaging with Pittsburgh compound B and florbetapir: comparing radiotracers and quantification methods. J Nucl Med. 2013;54(1):70–7. https://doi.org/10.2967/jnumed.112.109009.
27. Ng KP, Pascoal TA, Mathotaarachchi S, Therriault J, Kang MS, Shin M, et al. Monoamine oxidase B inhibitor, selegiline, reduces (18)F-THK5351 uptake in the human brain. Alzheimers Res Ther. 2017;9(1):25. https://doi.org/10.1186/s13195-017-0253-y.
28. Wu Y, Carson RE. Noise reduction in the simplified reference tissue model for neuroreceptor functional imaging. J Cereb Blood Flow Metab. 2002;22(12):1440–52. https://doi.org/10.1097/01.WCB.0000033967.83623.34.
29. Teng E, Ward M, Manser PT, Sanabria-Bohorquez S, Ray RD, Wildsmith KR, et al. Cross-sectional associations between [18F]GTP1 tau PET and cognition in Alzheimer's disease. Neurobiol Aging. 2019. Accepted.
30. Leuzy A, Chiotis K, Lemoine L, Gillberg PG, Almkvist O, Rodriguez-Vieitez E, et al. Tau PET imaging in neurodegenerative tauopathies-still a challenge. Mol Psychiatry. 2019. https://doi.org/10.1038/s41380-018-0342-8.

31. Gobbi LC, Knust H, Korner M, Honer M, Czech C, Belli S, et al. Identification of three novel radiotracers for imaging aggregated tau in Alzheimer's disease with positron emission tomography. J Med Chem. 2017;60(17):7350–70. https://doi.org/10.1021/acs.jmedchem.7b00632.
32. Barret O, Alagille D, Sanabria S, Comley RA, Weimer RM, Borroni E, et al. Kinetic modeling of the tau PET tracer (18)F-AV-1451 in human healthy volunteers and Alzheimer disease subjects. J Nucl Med. 2017;58(7):1124–31. https://doi.org/10.2967/jnumed.116.182881.
33. Shcherbinin S, Schwarz AJ, Joshi A, Navitsky M, Flitter M, Shankle WR, et al. Kinetics of the tau PET tracer 18F-AV-1451 (T807) in subjects with normal cognitive function, mild cognitive impairment, and Alzheimer disease. J Nucl Med. 2016;57(10):1535–42. https://doi.org/10.2967/jnumed.115.170027.